Evaluation of CMIP6 HighResMIP in simulating the annual cycle of tropical cyclone activity over the western North Pacific

Kuan-Chieh Chen[1], Chi-Cherng Hong[1*], Chih-Hua Tsou[2], and Ding-Rong Wu[3]

[1]Department of Earth and Life Science, University of Taipei, Taipei, Taiwan

[2]Department of Earth Sciences, National Taiwan Normal University, Taipei, Taiwan

[3]Department of Atmospheric Sciences, National Taiwan University, Taipei, Taiwan

For submission to *Geophysical Research Letters*

December 2023

*Corresponding author: Dr. Chi-Cherng Hong (cchong@utaipei.edu.tw; hong0202@gmail.com)

Department of Earth and Life Science, University of Taipei, No.1, Aiguo W. Rd., Zhongzheng Dist., Taipei City 100234, Taiwan (R.O.C.)

Key Points:

- Atmospheric and coupled general circulation models capture the number and genesis location of tropical cyclones over the annual cycle.
- Tropical cyclone numbers decreased less rapidly in atmospheric models than coupled models and observed data during monsoon retreat.
- This bias was due to an underestimation of the southward migration of the subtropical high ridge.

Abstract

Atmospheric general circulation models (AGCMs) and coupled general circulation models (CGCMs) in the High-Resolution Model Intercomparison Project (HighResMIP) were evaluated on their ability to simulate tropical cyclone (TC) activity in the western North Pacific over its annual cycle. Specifically, we examined these models' ability to simulate the south-north migration of mean TC genesis location. The results revealed that both types of models realistically captured TC numbers and the south-north migration of TC genesis locations in response to the annual cycle. However, TC number decreased less rapidly in the AGCMs than in both the CGCMs and observed data during the monsoon retreat period (after September). This bias was attributed to a cyclonic anomaly in the Philippine Sea in response to La Niña-like sea surface temperature (SST) differences between the AGCMs and the CGCMs. This cyclonic anomaly occurred when the northeasterly trade wind arose and was maintained through wind-evaporation-SST feedback.

Keywords: HighResMIP, tropical cyclone, annual cycle, subtropical high, WES feedback

Plain Language Summary

Tropical cyclone (TC) genesis locations in the western North Pacific (WNP) migrate from south to north over the annual cycle. Understanding the strengths and limitations of models in simulating this cycle is crucial to TC prediction. We used simulations from the High-Resolution Model Intercomparison Project (HighResMIP) to examine the accuracy of several models in simulating such migration. We found that the ensemble mean outputs of six atmospheric general circulation (AGCM) models and those of six coupled general circulation (CGCM) models realistically captured the TC numbers and meridional migration of TC genesis locations associated with the meridional migration of the WNP subtropical high ridge. However, TC number decreased less rapidly in the AGCMs than in both the CGCMs and observed data during the monsoon retreat period (after September). This bias stemmed from differences between the AGCMs and the CGCMs in simulating a low-tropospheric cyclonic anomaly in the Philippine Sea in response to La Niña-like sea surface temperatures. Because of these differences, TC genesis frequency in the AGCMs over the Philippine Sea was overestimated. The cyclonic anomaly appeared when a northeasterly trade wind arose and was maintained through positive feedback between wind, evaporation, and sea surface temperature.

1. Introduction

The western North Pacific (WNP) is the region in the tropics where most tropical cyclones (TCs) originate from, and TC activity in that area has a clear annual cycle (Lander, 1994; Chia & Ropelewski, 2002; Wang & Chan, 2002; Gilford et al., 2017; Sobel et al., 2021). Analysis of TC genesis locations in response to the annual cycle reveals a clear pattern of south-north migration. The ability of models to simulate the south-north movement of TC genesis location is closely related to the ability of models to simulate the intensity and landfall frequency of TCs (Camargo & Sobel, 2005; Zhang et al., 2012). Numerous studies have employed general circulation models (GCMs) to simulate and predict the annual cycle of TC activity (Camargo, 2013; Roberts et al., 2015, 2020a; Dwyer et al., 2015; Sharmila et al., 2020; Tang et al., 2022).

Studies have reported that models with higher horizontal resolution better simulate TC activity and TC number over the annual cycle (Manganello et al., 2012; Roberts et al., 2015, 2020a; Tang et al., 2022; Chen et al., 2023). The high-resolution global atmospheric model (HiRAM) and downscaling models from the Coupled Model Intercomparison Project (CMIP) phase 3 (CMIP3) and phase 5 (CMIP5) are able to capture the annual cycle of TC numbers in the WNP (Dwyer et al., 2015; Tsou et al., 2016). However, high-resolution downscaling models from CMIP3 and CMIP5 have been shown to underestimate TC numbers during the peak TC season (Dwyer et al., 2015). Tang et al. (2022) found that both uncoupled and coupled simulations in CMIP6 High-Resolution Model Intercomparison Project (HighResMIP) realistically captured the annual cycle of TC genesis. Their study also showed that coupled runs are more highly correlated with the observed annual cycle of TC numbers than uncoupled runs.

Most of the aforementioned studies have focused on the simulation of TC numbers over the annual cycle. However, few studies have investigated the accuracy of models in simulating the south-north movement of TC genesis locations and the effects of meridional migration of the WNP subtropical high (WNPSH) on this movement. In this study, we employed GCMs from CMIP6 HighResMIP to examine simulations of the annual TC cycle over the WNP. We focused on the climatology of TC numbers and locations, and the effects on TC location from large-scale environmental factors including the WNPSH.

2. Data and Methods

2.1 Data

The observed data for seasonal cycles over 1979-2008 were compared against model simulations on dynamic and thermodynamic characteristics. Data on atmospheric conditions were obtained from the National Centers for Environmental Prediction (NCEP) Climate Forecast System Reanalysis (CFSR) database with a 0.5° × 0.5° longitude-latitude resolution (Saha et al., 2010). Version 1 of the Met Office Hadley Centre Sea Ice and Sea Surface Temperature (HadISST1) dataset, which has a 1° × 1° longitude-latitude resolution, was used to obtain sea surface temperature (SST) (Rayner et al., 2003).

The observed TC data in the WNP were obtained from the Joint Typhoon Warning Center (JTWC). We only considered TCs with maximum wind speeds ≥ 35 knots (approximately 17.5 m s^{-1}). We defined TC genesis location as the position of the first data point recorded in the lifetime of a TC.

2.2 Model Simulations

We used models with higher horizontal resolution (25 to 50 km) from the

European Union Horizon 2020 project PRIMAVERA (https://www.climateurope.eu/primavera/) under the CMIP6 HighResMIP experimental protocol (Haarsma et al., 2016); these models were CMCC-CM2-VHR4 (Scoccimarro et al., 2017), CNRM-CM6-1-HR (Voldoire, 2019), EC-Earth3P-HR (EC-Earth, 2018), ECMWF-IFS-HR (Roberts et al., 2017), HadGEM3-GC31-HM (Roberts, 2017), and MPI-ESM1-2-XR (von Storch et al., 2017), as described in Table S1. Each GCM completed the atmospheric (highresSST-present; tier 1) and coupled (hist-1950; tier 2) runs during 1950-2014. The CMIP6 HighResMIP protocol and the simulation design of these six model groups are detailed in Haarsma et al. (2016) and Roberts et al. (2020a), respectively.

TC locations and tracks from model simulations were obtained using the objective feature-tracking algorithm "TRACK" (Hodges et al., 2017). This algorithm used data on 6-hour relative vorticity at 850, 700, and 600 hPa to track TCs on a common T63 spectral grid with warm-core criteria. More detecting criteria are described in Roberts et al. (2020a). Modeled TC data were accessed from the Centre for Environmental Data Analysis (Roberts et al., 2020a, 2020b).

2.3 Methods of Analysis

We applied a genesis potential index (GPI) based on the work of Murakami and Wang (2010) to explore the annual cycle of TC genesis in connection with large-scale environmental variations. The GPI is defined as:

$$\mathrm{GPI} = |10^5\eta|^{3/2}\left(\frac{\mathrm{RH}}{50}\right)^3\left(\frac{\mathrm{V_{pot}}}{70}\right)^3(1+0.1\mathrm{V_s})^{-2}\left(\frac{-\omega+0.1}{0.1}\right), \quad (1)$$

where η is the absolute vorticity at 850 hPa (s^{-1}), RH is the relative humidity at 600 hPa (%), V_{pot} is the maximum TC potential intensity (m s^{-1}), V_s is the magnitude of the vertical wind shear (m s^{-1}) between 850 and 200 hPa, and ω is the vertical

pressure velocity at 500 hPa (Pa s^{-1}).

To quantify the relative contributions of individual terms to total GPI difference, we followed Li et al. (2013) in considering the difference between the atmospheric GCM (AGCM) and coupled GCM (CGCM) values for each term but fixed the multiple of the remaining terms as the climatology in AGCM.

3. Results

3.1 Variation in TC Genesis Frequency Over the Annual Cycle

Figure 1 illustrates the annual cycles of TC numbers in the WNP. In the observed data, TC number increases substantially after June, peaks in August, and decreases noticeably after September (Figure 1a). All AGCMs and CGCMs realistically simulated the annual cycle of TC frequency except MPI-ESM1-2-XR (Figures 1b–1g). The underestimation of TC numbers in the MPI-ESM1-2-XR has been reported in earlier studies (Roberts et al., 2020a, 2020b; Tang et al., 2022). Because a multimodel ensemble mean may reduce the bias and uncertainty inherent in individual runs, we use the ensemble mean in the following analysis. For convenience, the ensembles of atmospheric runs and air-sea coupled runs are referred to as Ens-AGCM and Ens-CGCM, respectively. The MPI-ESM1-2-XR estimates were excluded from the ensemble mean due to their underestimation of TC numbers.

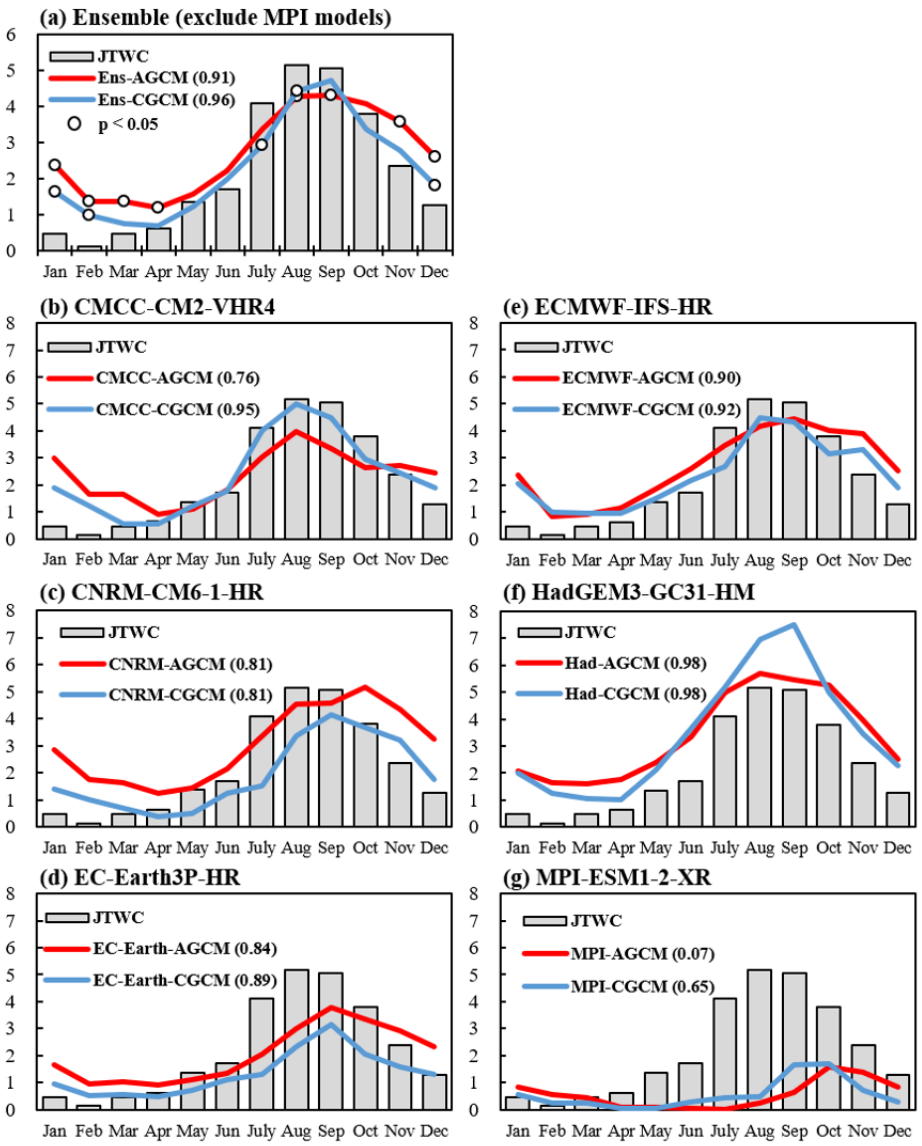

Figure 1. Comparisons of the climatology (1979-2008) of annual cycle of TC genesis numbers in the WNP between the observed data (gray bar), CMIP6 HighResMIP AGCM (red line) and CGCM (blue line) simulations from (a) the ensemble mean excluding MPI-ESM1-2-XR simulations (referred to as Ens-AGCM and Ens-CGCM), and (b-g) individual models. The numbers within parentheses indicate the temporal correlation coefficient between simulation and observed data. The white circles in (a) indicate that the difference in TC numbers between model simulation and observed data is statistically significant.

The annual cycle of TC frequency was successfully captured by the ensemble mean (Figure 1a). Ens-AGCM and Ens-CGCM had temporal correlation coefficients larger than 0.9 in relation to the observed data. During the development stage of the WNP monsoon (June-September), the Ens-AGCM and the Ens-CGCM closely fit the observed TC numbers. However, the number of TCs decreased more gradually in the

Ens-AGCM than in both the Ens-CGCM and observed data during the retreat stage of the WNP monsoon (after September).

Figure 2 depicts the spatial distribution of TC genesis frequency and mid-tropospheric geopotential height during the typhoon season. In June and July, most TCs formed in the Philippine Sea (Figure 2a). In response to the annual cycle, the TC genesis locations extended eastward and migrated northward to the south of Japan during August-September (Figure 2d). The locations migrated southward to the south of 20°N in October-November (Figure 2g). The meridional migrations of TC genesis locations were primarily controlled by the location of the ridge of the WNPSH (WNP-SHR; see the dashed line in Figure 2), which moved northward and southward in response to the period of monsoon development and retreat, respectively. That is, the TCs frequently formed south of the WNP-SHR (Figures 2a, 2d, and 2g). These results indicate that the location of the WNP-SHR plays a crucial role in determining the north extension of TC genesis locations.

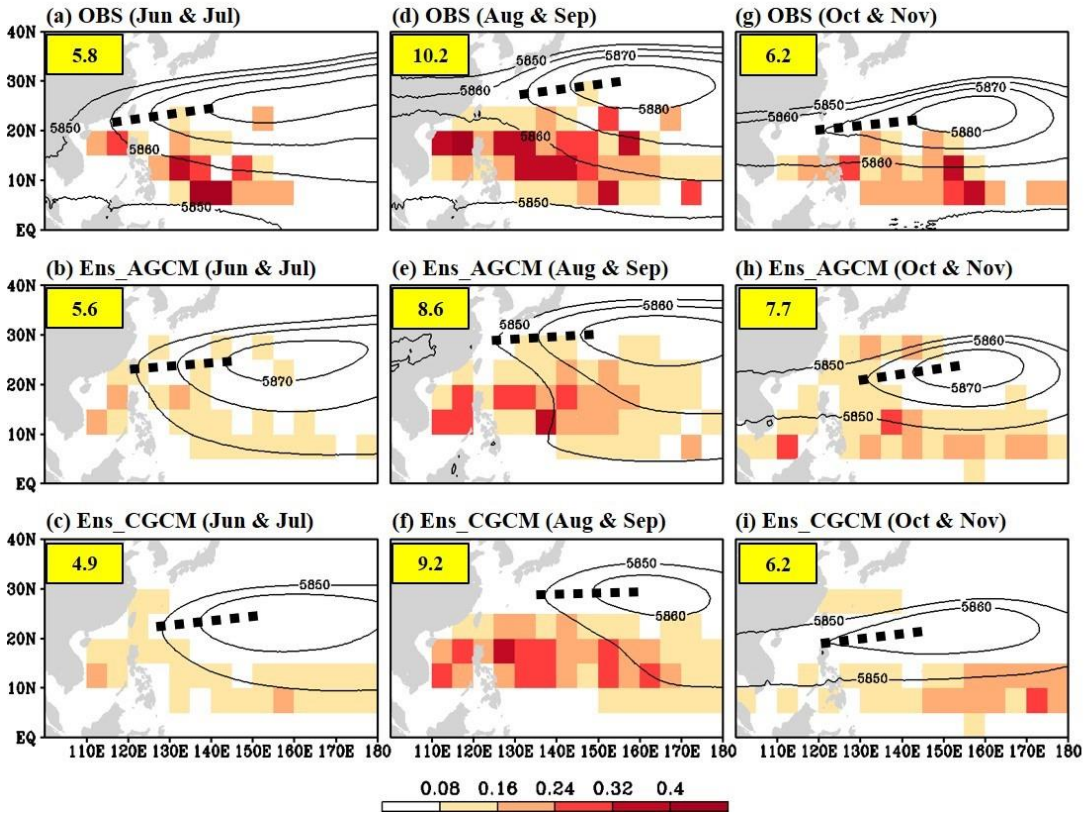

Figure 2. Climatology of TC formation frequency (numbers year^{-1}; shaded) and 500-hPa geopotential height (m; contour) with a ridge (black dotted line) during June-July for (a) observation, (b) Ens-AGCM, and (c) Ens-CGCM. (d-f) and (g-i) same as (a-c) except for during August-September and October-November, respectively. The number in each picture indicates the TC count (per year) in the WNP.

Overall, both the Ens-AGCM and the Ens-CGCM reasonably simulated the meridional migration of the WNP-SHR and TC genesis locations in response to the annual cycle (Figures 2b–2c, 2e–2f, and 2h–2i). For the June-July period, the Ens-AGCM simulated the TC genesis numbers and locations more accurately than the Ens-CGCM (Table S2). However, the Ens-AGCM had a clear eastward shift in the WNP-SHR during October-November (compare the dashed lines in Figures 2h and 2g). This bias weakened the strength of the WNP-SHR in the Philippine Sea. TC genesis numbers were thus overestimated (underestimated) north (south) of 20°N in the Ens-AGCM (Figure 2h). By contrast, the Ens-CGCM realistically captured the southward and westward retreat of the WNP-SHR (Figure 2i). The simulation of TC genesis location and number was more accurate during the period of monsoon retreat.

3.2 GPI Analysis

A GPI analysis was applied to investigate the effects of large-scale thermodynamic and dynamic factors on the discrepancy in TC genesis numbers and locations between the models and observed data. Figure S1 presents the climatologies of GPI and TC genesis frequency in the observed data and simulations for comparison. Overall, the GPIs closely fit the data for TC genesis, although the simulated GPIs were overestimated due to an overestimation in the monsoon trough. The meridional migration of the GPIs in response to the seasonal cycle also was reasonably simulated. These results indicate that GPIs are indeed useful indicators of the seasonal variation of TC frequency in the WNP.

Because the Ens-AGCM was most inaccurate in simulating the annual cycle of

TC activity (number and location) during the monsoon retreat, we focused on the October-November period in our GPI analysis. Figure 3a illustrates the differences between the Ens-AGCM and the Ens-CGCM in total GPI and TC genesis frequency. These distributions of GPI and TC genesis frequency differed similarly and exhibited an east-west dipole structure. That is, the Ens-AGCM overestimated (underestimated) the GPI west (east) of 150°E compared with the Ens-CGCM. This overestimation of GPIs over the Philippine Sea resulted in a more gradual decrease in TC genesis number compared with the Ens-CGCM during the monsoon retreat (Figure 1a). The GPI includes five terms, and the relative contribution of each term to the total GPI difference was estimated per the method of Li et al. (2013). Our estimate revealed that mid-tropospheric relative humidity dominated the GPI difference and that upward motion played a secondary role (Figure 3b). The contributions of lower-level vorticity, maximum potential intensity, and vertical wind shear were not significant. Mid-tropospheric relative humidity, vertical motion, and the eastward shift of the WNP-SHR (Figures 2h and 2i) worked in conjunction to create favorable conditions for TC genesis. This accounts for the less rapid decrease in TC activity during October-November.

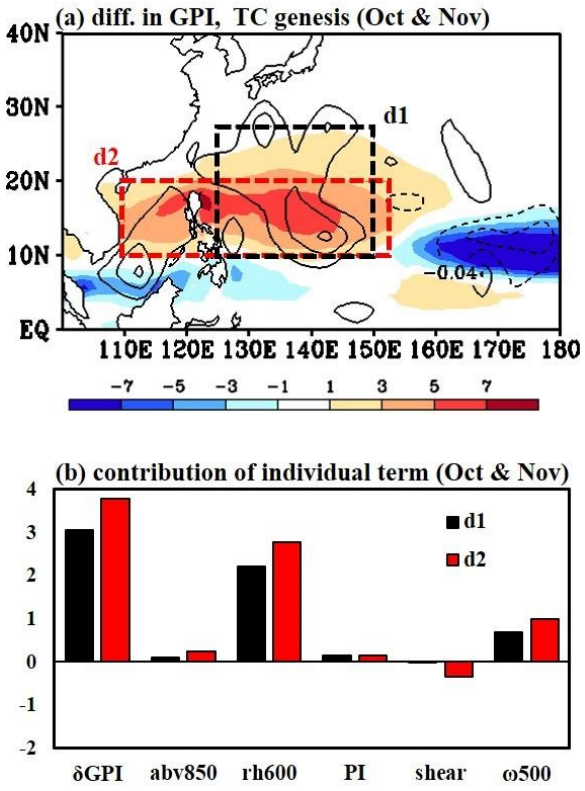

Figure 3. The difference between the Ens-AGCM and Ens-CGCM simulations (Ens-AGCM minus Ens-CGCM) during October-November in (a) GPI (shaded) and TC genesis frequency (numbers year^{-1}; contour), and (b) the relative contribution of individual terms of GPI over the d1 and d2 domains [black and red boxes in (a), respectively].

3.3 Causes of Simulation Bias in the Ens-AGCM

As indicated in Figure 2, TC genesis numbers were underestimated (overestimated) during August-September (October-November) in the Ens-AGCM. This explains the bias of the Ens-AGCM in simulating the annual cycle of TC frequency. The possible causes for this bias are discussed in the following sections.

a. Atmospheric circulation in response to La Niña-like SST

Figure 4 presents the differences in SST and the 850 hPa streamfunction between the Ens-AGCM and the Ens-CGCM (Ens-AGCM minus Ens-CGCM) for August-September and October-November. The SST difference has a La Niña-like pattern that persists through the summer to the autumn. Because the Ens-AGCM was forced by the observed SST as the lower boundary condition, the La

Niña-like SST reflects an El Niño-like SST bias in the coupled models, a common feature seen in CMIP6 simulations (Zhang et al., 2023). In response to the La Niña-like SST, a Gill-type large-scale anticyclonic circulation anomaly was identified in the subtropical Pacific in the Northern Hemisphere during August-September (Figure 4a). This anticyclonic anomaly weakened the WNP monsoon trough, which in turn suppressed TC genesis. These unfavorable conditions contributed to the Ens-AGCM's underestimation of TC numbers in summer compared with the estimates given by the Ens-CGCM (Figures 2e–2f). The anticyclonic anomaly in the WNP persisted for the entire monsoon season, with the center shifting east in autumn (Figure 4b). Additionally, a cyclonic anomaly moved eastward from the Indian Ocean to the Philippine Sea during October-November. The cyclonic anomaly provided favorable large-scale conditions for TC genesis. Consequently, the decrease in TC numbers during October-November estimated by the Ens-AGCM was more gradual than the decrease seen in both the observed data and Ens-CGCM.

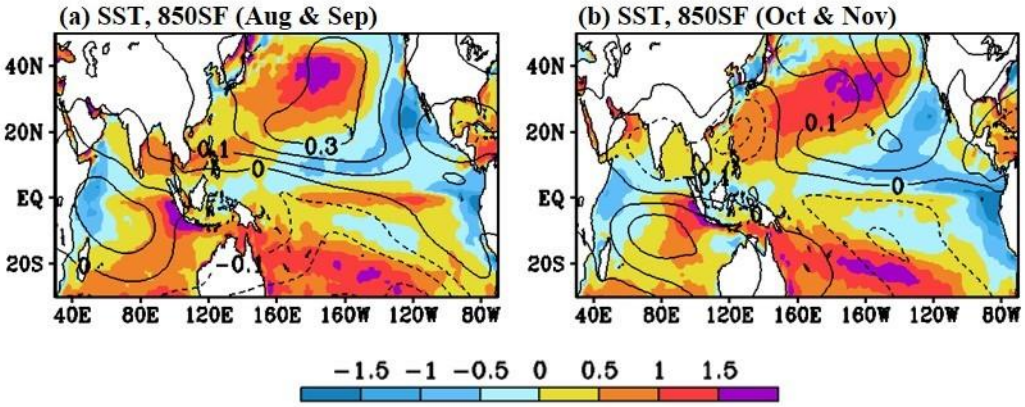

Figure 4. The difference in the SST (°C; shaded) and 850-hPa stream function (10^7 m^2 s^{-1}; contour) between the Ens-AGCM and Ens-CGCM simulations (Ens-AGCM minus Ens-CGCM) during (a) August-September, and (b) October-November.

b. Season-dependent local air-sea interaction

Wang et al. (2000) uncovered the mechanism of local air-sea interaction to explain

the establishment and maintenance of anticyclonic anomalies in the Philippine Sea during the mature phase of El Niño. The atmospheric response in the Philippine Sea during October-November reflected the working of this mechanism. During August-September, the anticyclonic anomaly in the Philippine Sea was part of a large-scale anticyclonic anomaly in response to La Niña-like SST (Figures 4a and S2a). During October-November, this Gill-type anticyclonic anomaly moved eastward, and the Philippine Sea was covered by a cyclonic anomaly that moved from the Indian Ocean. The southwesterly associated with this cyclonic anomaly was against the northeasterly prevailing wind in the central-western tropical Pacific (Figures 4b and S2b). The cyclonic anomaly weakened the northeasterly trade wind, which warmed the SST in the Philippine Sea and cooled the SST along the coast of East China through wind-evaporation-SST (WES) feedback (Wang et al., 2000). This feedback created an east-west-distributed SST anomaly extending along the East China coast and the Philippine Sea. The east-west SST anomaly itself created a circulation anomaly that maintained the cyclonic anomaly in the Philippine Sea.

Figure S3 shows the annual cycle of SST and surface flux averaged in the regions where WES feedback occurred. The latent heat flux exchange cools the SST, and its effect increases from summer to winter in response to the establishment of a prevailing northeasterly wind (Wang et al., 2000). During October-November, the magnitude of latent heat is close to that of the incoming shortwave radiation, and the SST in this region rapidly decreased. An anticyclonic anomaly accompanied by an east-west-distributed SST anomaly was identified in the Philippine Sea and along the East China coast in the Ens-GCM compared with the results in the Ens-AGCM

298 (upper-left panel in Fig. S3). The northeasterly (southwesterly) associated with this
299 anticyclonic anomaly was in phase (against) the prevailing wind. The
300 east-west-distributed SST anomaly and the accompanying anticyclonic anomaly were
301 sustained by the air-sea coupling process of WES positive feedback.

302 Mean TC genesis locations were strongly influenced by the WNP-SHR, which
303 migrated northward to Japan in summer and returned to the South China Sea in
304 autumn. The southward migration of the WNP-SHR in autumn suppressed TC genesis
305 and caused TCs to only occur south of 20°N. The lack of air-sea interaction in the
306 Ens-AGCM, combined with the seasonal cycle, caused the models to underestimate
307 the WNP-SHR. This underestimation gave rise to an overestimation of the GPI and
308 TC numbers in the Philippine Sea (Figure 3). Consequently, the annual cycle of TC
309 numbers in the Ens-AGCM did not exhibit the same rapid decrease seen in both the
310 observed data and Ens-CGCM.

311

312 **4. Conclusion and Remarks**

313 This study evaluated the performance of HighResMIP models in simulating TC
314 activity over its annual cycle, including the number and location of TCs, in the WNP.
315 The possible causes of biases in simulating TC activity were addressed. The results
316 are summarized as follows (Figure 5).

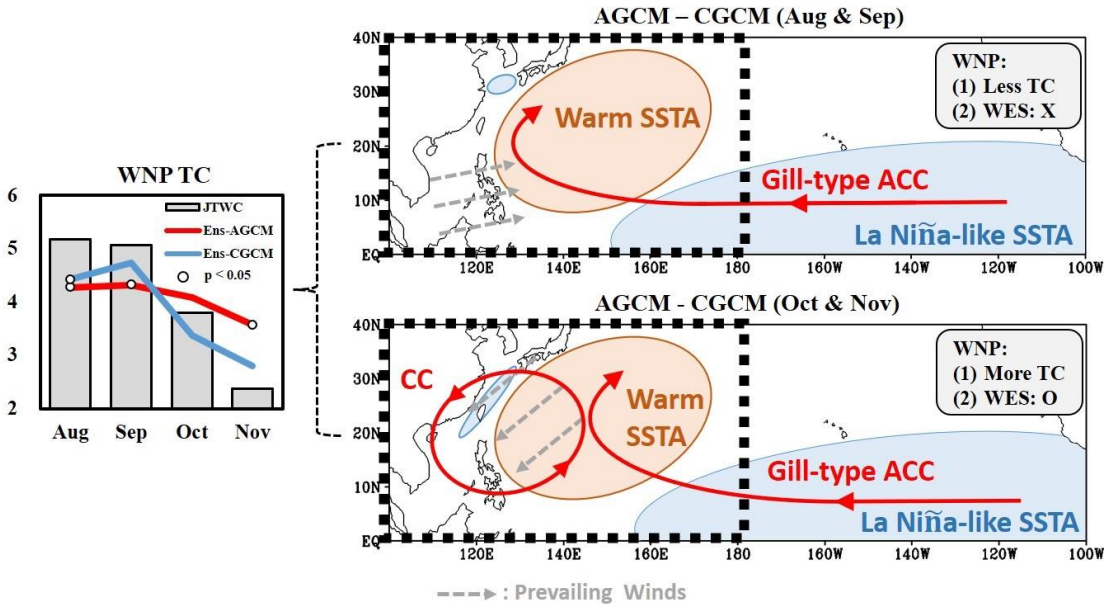

Figure 5. Schematic diagram illustrates the causes of bias for TC genesis frequency simulated by Ens-AGCM in the WNP (black dotted boxes) during the monsoon development and retreat periods through a comparison between the Ens-AGCM and Ens-CGCM.

1. The Ens-AGCM and the Ens-CGCM reasonably simulated the annual cycle of TC numbers. However, TC numbers were underestimated (overestimated) during the monsoon development (retreat) in the Ens-AGCM compared with the observed data and with the Ens-CGCM. This bias caused the Ens-AGCM to fail to simulate a rapid decrease in TC number after September.
2. The Ens-AGCM and the Ens-CGCM both captured the meridional migration of the WNP-SHR in response to the seasonal cycle. Nevertheless, the WNP-SHR in the Ens-AGCM exhibited a west (east) shift bias during August-September (October-November). This bias resulted in an underestimation (overestimation) of TC numbers for August-September (October-November). The mean locations of TC genesis also shifted substantially northward in October-November due to the eastward shift of the WNP-SHR.
3. The GPI analysis revealed that the overestimations of GPI and TC numbers over the South China Sea and the Philippine Sea (10°-20°N, 110°-150°E) during

October-November in the Ens-AGCM were due to overestimations of mid-tropospheric relative humidity and upward motion. The underestimations of the GPI between 10°N and 20°N during August-September were due to underestimations of mid-tropospheric relative humidity and low-tropospheric vorticity (Figure S4).

4. The differences in simulations of the annual cycle of TC numbers between runs using coupled and uncoupled models can be explained by a large-scale circulation anomaly over the WNP in response to a La Niña-like SST difference between the Ens-AGCM and the Ens-CGCM (Figure 5). The Gill-type anticyclonic anomaly in response to the La Niña-like SST dominated large-scale circulation in the WNP during August-September. The anticyclonic anomaly shifted eastward during October-November. During this period, a cyclonic anomaly occurred in the Philippine Sea and was maintained through local air-sea interaction, a WES positive feedback mechanism (Wang et al., 2000). This cyclonic anomaly favored TC activity and caused an overestimation of TC numbers in the Philippine Sea.

This study indicates that the HighResMIP simulations reasonably capture the annual cycle of TC activity in the WNP. However, the Ens-AGCM tends to overestimate the atmospheric response to prescribed SST (Lau & Ploshay, 2009). That is, a positive SST anomaly is expected to cause above-normal precipitation (Figure S5). However, the SST-precipitation relationship is usually negatively correlated in the WNP during the boreal summer monsoon (Wang et al., 2005). An anticyclonic anomaly with below-normal rainfall may cause a positive SST anomaly through associated large-scale subsidence. However, deep convection is usually accompanied by a negative SST anomaly due to cloud-radiation-SST feedback (Ramanathan &

Collins, 1991; Li et al., 2000; Hong et al., 2008). These processes were not successfully captured in the AGCMs, causing significant bias in the Ens-AGCM in simulating the annual cycle of TC activity.

Since only an ensemble of five models might be doubtful, the ensemble size extending to seven (add ECMWF-IFS-LR and MPI-ESM1-2-XR) was analyzed, suggesting the robustness of discrepancy in the annual cycle of TC frequency (Figure S6). In addition to current climatological conditions, changes in the annual cycle of TC activity in future projection under global warming were investigated. Space constraints disallow us from presenting these predictions here; we aim to present them in a future manuscript.

Our comparison between the atmospheric and coupled runs of the CMIP6 HighResMIP highlights the importance of the air-sea interaction in capturing the meridional migration of the WNP-SHR over the annual cycle. Realistic simulation of the WNP-SHR is crucial to the accuracy of a model in simulating the annual cycle of TC activity in the WNP. These results help us better predict seasonal TCs and understand the complex interactions among SST, atmospheric circulation, and TC genesis over the annual cycle.

Conflicts of Interest

The authors declare no conflicts of interest.

Data Availability Statement

The observed monthly atmospheric conditions and sea surface temperature were obtained from the National Centers for Environmental Prediction (NCEP) Climate Forecast System Reanalysis (https://rda.ucar.edu/datasets/ds093.2/) and the Met

Office Hadley Centre Sea Ice and Sea Surface Temperature version 1 (https://www.metoffice.gov.uk/hadobs/hadisst/data/download.html), respectively. The observed tropical cyclone data in the western North Pacific were obtained from the Joint Typhoon Warning Center (https://www.metoc.navy.mil/jtwc/jtwc.html?western-pacific). The model outputs from CMIP6 HighResMIP were obtained from the Earth System Grid Federation nodes (https://esgf-node.llnl.gov/projects/cmip6/). The tropical cyclone tracks detected by the TRACK algorithm were obtained from the Centre for Environmental Data Analysis (https://data.ceda.ac.uk/badc/highresmip-derived/data/storm_tracks/TRACK).

Acknowledgments

The analysis described in this paper was supported by the Ministry of Science and Technology (MOST), Taiwan, under grant numbers 112-2811-M-845-001 and 111-2111-M-845-001. We are grateful to Professor Tim Li for his valuable comments. We also wish to express our gratitude to Mr. HC Liang for his assistance in downloading the model outputs used. This manuscript was edited by Wallace Academic Editing.

References

Camargo, S. J. (2013). Global and Regional Aspects of Tropical Cyclone Activity in the CMIP5 Models. *Journal of Climate, 26*(24), 9880-9902. https://doi.org/10.1175/JCLI-D-12-00549.1

Camargo, S. J., & Sobel, A. H. (2005). Western North Pacific Tropical Cyclone Intensity and ENSO. *Journal of Climate, 18*(15), 2996-3006. https://doi.org/10.1175/JCLI3457.1

Chen, K. C., Tsou, C. H., Hong, C. C., Hsu, H. H., & Tu, C. Y. (2023). Effect of model resolution on simulation of tropical cyclone landfall in East Asia based on a comparison of 25- and 50-km HiRAMs. *Climate Dynamics, 61*(5-6), 2085-2101. https://doi.org/10.1007/s00382-023-06668-z

Chia, H. H., & Ropelewski, C. F. (2002). The Interannual Variability in the Genesis Location of Tropical Cyclones in the Northwest Pacific. *Journal of Climate, 15*(20), 2934-2944. https://doi.org/10.1175/1520-0442(2002)015<2934:TIVITG>2.0.CO;2

Dwyer, J. G., Camargo, S. J., Sobel, A. H., Biasutti, M., Emanuel, K. A., Vecchi, G. A., et al. (2015). Projected Twenty-First-Century Changes in the Length of the Tropical Cyclone Season. *Journal of Climate, 28*(15), 6181-6192. https://doi.org/10.1175/JCLI-D-14-00686.1

EC-Earth Consortium. (2018). EC-Earth-Consortium EC-Earth3P-HR model output prepared for CMIP6 HighResMIP. https://doi.org/10.22033/ESGF/CMIP6.2323

Gilford, D. M., Solomon, S., & Emanuel, K. A. (2017). On the Seasonal Cycles of Tropical Cyclone Potential Intensity. *Journal of Climate, 30*(16), 6085-6096. https://doi.org/10.1175/JCLI-D-16-0827.1

Haarsma, R. J., Roberts, M. J., Vidale, P. L., Senior, C. A., Bellucci, A., Bao, Q., et al. (2016). High Resolution Model Intercomparison Project (HighResMIP v1.0) for CMIP6. *Geoscientific Model Development*, 9, 4185–4208. https://doi.org/10.5194/gmd-9-4185-2016

Hodges, K., Cobb, A., & Vidale, P. L. (2017). How well are tropical cyclones represented in reanalysis datasets?. *Journal of Climate, 30*(14), 5243–5264. https://doi.org/10.1175/JCLI-D-16-0557.1

Hong, C. C., Li, T., LinHo, & Kug, J. S. (2008). Asymmetry of the Indian Ocean Dipole. Part I: Observational Analysis. *Journal of Climate, 21*(18), 4834-4848. https://doi.org/10.1175/2008JCLI2222.1

Lander, M. A. (1994). An Exploratory Analysis of the Relationship between Tropical Storm Formation in the Western North Pacific and ENSO. *Monthly Weather Review, 122*(4), 636-651. https://doi.org/10.1175/1520-0493(1994)122<0636:AEAOTR>2.0.CO;2

Lau, N. C., & Ploshay, J. J. (2009). Simulation of synoptic- and subsynoptic-scale phenomena associated with the East Asian summer monsoon using a high-resolution GCM. *Monthly Weather Review, 137*(1), 137-160. https://doi.org/10.1175/2008MWR2511.1

Li, T., Hogan, T. F., & Chang, C. P. (2000). Dynamic and Thermodynamic Regulation of Ocean Warming. *Journal of the Atmospheric Sciences, 57*(20), 3353-3365. https://doi.org/10.1175/1520-0469(2000)057<3353:DATROO>2.0.CO;2

Li, Z., Yu, W., Li, T., Murty, V. S. N., & Tangang, F. (2013). Bimodal Character of Cyclone Climatology in the Bay of Bengal Modulated by Monsoon Seasonal

Cycle. *Journal of Climate*, *26*(3), 1033-1046. https://doi.org/10.1175/JCLI-D-11-00627.1

Manganello, J. V., Hodges, K. I., Kinter, J. L., III, Cash, B. A., Marx, L., Jung, T., et al. (2012). Tropical Cyclone Climatology in a 10-km Global Atmospheric GCM: Toward Weather-Resolving Climate Modeling. *Journal of Climate, 25*(11), 3867-3893. https://doi.org/10.1175/JCLI-D-11-00346.1

Murakami, H., & Wang, B. (2010). Future Change of North Atlantic Tropical Cyclone Tracks: Projection by a 20-km-Mesh Global Atmospheric Model. *Journal of Climate, 23*(10), 2699-2721. https://doi.org/10.1175/2010JCLI3338.1

Ramanathan, V., & Collins, W. (1991). Thermodynamic regulation of ocean warming by cirrus clouds deduced from observations of the 1987 El Niño. *Nature*, 351, 27-32. https://doi.org/10.1038/351027a0

Rayner, N. A., Parker, D. E., Horton, E. B., Folland, C. K., Alexander, L. V., Rowell, D. P., et al. (2003). Global analyses of sea surface temperature, sea ice, and night marine air temperature since the late nineteenth century. *Journal of Geophysical Research: Atmospheres*, 108, 4407. https://doi.org/10.1029/2002JD002670

Roberts, C. D., Senan, R., Molteni, F., Boussetta, S., & Keeley, S. (2017). ECMWF ECMWF-IFS-HR model output prepared for CMIP6 HighResMIP. https://doi.org/10.22033/ESGF/CMIP6.2461

Roberts, M. (2017). MOHC HadGEM3-GC31-HM model output prepared for CMIP6 HighResMIP. https://doi.org/10.22033/ESGF/CMIP6.446

Roberts, M. J., Camp, J., Seddon, J., Vidale, P. L., Hodges, K., Vannière, B., et al. (2020a). Impact of model resolution on tropical cyclone simulation using the HighResMIP–PRIMAVERA multimodel ensemble. *Journal of Climate, 33*(7), 2557-2583. https://doi.org/10.1175/JCLI-D-19-0639.1

Roberts, M. J., Camp, J., Seddon, J., Vidale, P. L., Hodges, K., Vannière, B., et al. (2020b). Projected future changes in tropical cyclones using the CMIP6 HighResMIP multimodel ensemble. *Geophysical Research Letters*, 47. https://doi.org/10.1029/2020GL088662

Roberts, M. J., Vidale, P. L., Mizielinski, M. S., Demory, M., Schiemann, R., Strachan, J., et al. (2015). Tropical Cyclones in the UPSCALE Ensemble of High-Resolution Global Climate Models. *Journal of Climate, 28*(2), 574-596. https://doi.org/10.1175/JCLI-D-14-00131.1

Saha, S., Moorthi, S., Pan, H., Wu, X., Wang, J., Nadiga, S., et al. (2010). The NCEP Climate Forecast System Reanalysis. *Bulletin of the American Meteorological Society, 91*(8), 1015-1058. https://doi.org/10.1175/2010BAMS3001.1

Scoccimarro, E., Bellucci, A., & Peano, D. (2017). CMCC CMCC-CM2-VHR4 model output prepared for CMIP6 HighResMIP. https://doi.org/10.22033/ESGF/CMIP6.1367

Sharmila, S., Walsh, K. J. E., Thatcher, M., Wales, S., & Utembe, S. (2020). Real World and Tropical Cyclone World. Part I: High-Resolution Climate Model Verification. *Journal of Climate*, *33*(4), 1455-1472. https://doi.org/10.1175/JCLI-D-19-0078.1

Sobel, A. H., Wing, A. A., Camargo, S. J., Patricola, C. M., Vecchi, G. A., Lee, C. Y., & Tippett, M. K. (2021). Tropical cyclone frequency. *Earth's Future*, 9, e2021EF002275. https://doi.org/10.1029/2021EF002275

Tang, Y., Huangfu, J., Huang, R., & Chen, W. (2022). Simulation and Projection of Tropical Cyclone Activities over the Western North Pacific by CMIP6 HighResMIP. *Journal of Climate*, *35*(23), 7771-7794. https://doi.org/10.1175/JCLI-D-21-0760.1

Tsou, C. H., Huang, P. Y., Tu, C. Y., Chen, C. T., Tzeng, T. P., & Cheng, C. T. (2016). Present simulation and future typhoon activity projection over Western North Pacific and Taiwan/East coast of China in 20-km HiRAM climate model. *Terrestrial, Atmospheric and Oceanic Sciences*, *27*(5), 687-703. https://doi.org/10.3319/TAO.2016.06.13.04

Voldoire, A. (2019). CNRM-CERFACS CNRM-CM6-1-HR model output prepared for CMIP6 HighResMIP. https://doi.org/10.22033/ESGF/CMIP6.1387

von Storch, J.-S., Putrasahan, D., Lohmann, K., Gutjahr, O., Jungclaus, J., Bittner, M., et al. (2017). MPI-M MPI-ESM1.2-XR model output prepared for CMIP6 HighResMIP. https://doi.org/10.22033/ESGF/CMIP6.10290

Wang, B., & Chan, J. C. L. (2002). How Strong ENSO Events Affect Tropical Storm Activity over the Western North Pacific. *Journal of Climate, 15*(13), 1643-1658.https://doi.org/10.1175/1520-0442(2002)015<1643:HSEEAT>2.0.CO;2

Wang, B., Ding, Q., Fu, X., Kang, I. S., Jin, K., Shukla, J., & Doblas-Reyes, F. (2005). Fundamental challenge in simulation and prediction of summer monsoon rainfall. *Geophysical Research Letters*, *32*(15), L15711. https://doi.org/10.1029/2005GL022734

Wang, B., Wu, R. G., & Fu, X. H. (2000). Pacific-East Asian teleconnection: How does ENSO affect East Asian climate? *Journal of Climate, 13*(9), 1517–1536. https://doi.org/10.1175/1520-0442(2000)013<1517:PEATHD>2.0.CO;2

Zhang, Q., Liu, B., Li, S., & Zhou, T. (2023). Understanding models' global sea surface temperature bias in mean state: From CMIP5 to CMIP6. *Geophysical*

529 *Research Letters*, 50, e2022GL100888.
530 https://doi.org/10.1029/2022GL100888
531 Zhang, W., Graf, H., Leung, Y., & Herzog, M. (2012). Different El Niño Types and
532 Tropical Cyclone Landfall in East Asia. *Journal of Climate, 25*(19),
533 6510-6523. https://doi.org/10.1175/JCLI-D-11-00488.1